Chinese Physics Letters

LETTER

Universal Scaling and Implications of the Apparent Anomalous Hall Voltage of Magnetic Layer with an Adjacent Conducting Layer

Cite as: Zhihao Yan *et al*. 2026 *Chin. Phys. Lett.* **43** 110707

DOI CSTR

Recommended Articles

Pressure-Tuned Intrinsic Anomalous Hall Conductivity in Kagome Magnets RV$_6$Sn$_6$ (R = Gd, Tb)

Xiangming Kong *et al*.
Chin. Phys. Lett. **41**, (2024)

Uncovering the Magnetization Multipolar Anisotropy of the Anomalous Hall Effect in Conventional Ferromagnets

Wenzhi Peng *et al*.
Chin. Phys. Lett. **43**, 060704 (2026)

Pressure-Enhanced Intrinsic Anomalous Hall Conductivity in the Kagome Ferrimagnet TbMn$_6$Sn$_6$

Hao Sun *et al*.
Chin. Phys. Lett. **43**, 030704 (2026)

Large Anomalous Hall Conductivity in Quasi-One-Dimensional Geometrically Frustrated Metal Pr$_3$MnBi$_5$

Xinyao Li, Feihong Guan, Xinhang Shan, Xiangde Zhu, Wei Ning, and Mingliang Tian
Chin. Phys. Lett. **43**, 040702 (2026)

Quantized Anomalous Hall Resistivity in Epitaxial MnBi$_2$Te$_4$ Thin Films on Ultrathin Cr$_2$Ge$_2$Te$_6$ Films

Yang Chen *et al*.
Chin. Phys. Lett. **43**, 080701 (2026)

Breakthrough in a Century-Old Paradigm: Multipolar Anisotropy of the Anomalous Hall Effect

Lei Wang, and Ke Xia
Chin. Phys. Lett. **43**, 070703 (2026)

A series journal of Chinese Physical Society distributed by IOP Publishing

Chinese Physics Letters

Chin. Phys. Lett. **43** 110707 (2026)

LETTER

DOI: 10.1088/0256-307X/43/11/110707
CSTR: 32039.14.0256-307X.43.11.110707

Universal Scaling and Implications of the Apparent Anomalous Hall Voltage of Magnetic Layer with an Adjacent Conducting Layer

Zhihao Yan[1,2], Qianbiao Liu[1], Zhengxiao Li[1,2], and Lijun Zhu[1,2,*]

[1]State Key Laboratory of Semiconductor Physics and Chip Technologies, Institute of Semiconductors, Chinese Academy of Sciences, Beijing 100083, China
[2]Center of Materials Science and Optoelectronics Engineering, University of Chinese Academy of Sciences, Beijing 100049, China

[*]Corresponding author. Email: ljzhu@semi.ac.cn

The anomalous Hall voltage of magnetic heterostructures plays a key role via the interplay with a variety of spintronic effects. Under a given electric field (E), the anomalous Hall voltage of a magnetic layer should remain unaffected by adjacent layers unless the latter could modify or contribute to the anomalous Hall conductivity. In this Letter, we report the observation, universality, mechanism, and impacts of the dramatic scaling of the apparent anomalous Hall voltage per electric field (V_{AH}/E) of magnetic heterostructures with the thickness and resistivity of the nonmagnetic conducting layers by combining transport experiments, analytical derivation, and finite-element analyses. We identify that the scaling arises simply from the misreading of the invariant internal anomalous Hall voltage due to the series-resistor effect of the magnetic and nonmagnetic layers within the magnetic heterostructures. The scaling remains strong regardless of the strengths of the spin–orbit torques and spin and orbital Hall conductivities of the normal metals, suggesting that interfacial angular momentum transport plays a minimal role in the anomalous Hall effect. We also show that the harmonic Hall voltage analyses of magnetic heterostructures remain robust against the considerable underestimation of the anomalous Hall voltage and other transverse voltages due to the series-resistor effect. These findings provide crucial information for understanding a variety of spintronic experiments involving the anomalous Hall and other transverse voltages.

Introduction

The anomalous Hall effect of magnetic heterostructures has been playing a key role in spintronics. First of all, the anomalous Hall voltage (V_{AH}) under a given electric field E [Fig. 1(a)], or the correlated anomalous Hall resistance (=V_{AH}/I_{tot}, with I_{tot} being the total current in the heterostructures), has been widely utilized as the readout for magnetic fields [1–5], magnetization states [6–9], magnetic domains [10,11], magnetic skyrmions [12–14], and interfacial spin–orbit coupling [15,16]. Furthermore, V_{AH} correlates the first- and second-harmonic Hall voltages ($V_{1\omega}$ and $V_{2\omega}$) to the dampinglike spin–orbit torque (SOT) in normal metal/ferromagnetic metal (NM/FM) bilayers [17–21], superlattices [22–24], magnetic single layers [25–28], synthetic antiferromagnets [29–31], antiferromagnet/NM bilayers [32,33], or ferrimagnet/NM bilayers [34,35]. V_{AH} can also monitor the magnetization-dependent interfacial scattering of angular momentum and electrons in unusual magnetoresistance experiments [36] and indicate the magnetization tilting or switching induced by magnetic fields [37–39], the Dzyaloshinskii–Moriya interaction [40–42], or spin currents [38, 43,44].

It has been well established that V_{AH} of a magnetic single layer originates from the band structure (intrinsic mechanism) and impurity scattering (side jump and skew scattering) [45–51]. V_{AH} of a magnetic single layer (we note as $V_{AH,0}$) under a given E is principally given by

$$V_{AH,0}/E = \sigma_{AH} W/\sigma_{FM}, \quad (1)$$

where σ_{AH}, W, and σ_{FM} are the anomalous Hall conductivity, the width, and the longitudinal conductivity of the magnetic layer, respectively. As indicated by Eq. (1), $V_{AH,0}/E$ of a magnetic layer should be independent of any adjacent layers unless the latter could significantly modify or contribute to σ_{AH}. For investigating novel physics, $V_{AH,0}/E$ is superior to V_{AH}/I_{tot} since V_{AH}/I_{tot} varies strongly due mainly to the parallel-resistor shunting effect accompanied by other entangling effects.

So far, it has remained a crucial open question as to whether and how V_{AH}/E of a magnetic layer within spintronic devices should be generally affected by the adjacent NMs. There has been no experimental demonstration of any variation of V_{AH}/E of NM/FM bilayers with NM thicknesses (d). Spin current from NMs was speculated to strongly modify [52–56] or even overwhelm [57] V_{AH}/I_{tot} of the NM/FM bilayers. Previous experiments suggested a strong reduction of V_{AH}/I_{tot} with increasing d (i.e., the anomalous Hall resistance) in Fe/Cu bilayers [58] and Ta/Pt/Co/Al/Pt multilayers [52], while the dominance of current shunting into the NM layers (parallel-resistor effect) prevented precise identification of other entangling mechanisms. Electric symmetry breakings induced by the contacts have demonstrated to enable efficient z spin generation from polycrystalline and amorphous heavy metals and all-electric switching of perpendicular magnetization [59–61], but its influence on the V_{AH} measurements has remained yet to study. Precise understanding of the magnitude of V_{AH} is critical not only for analyses of a variety of spin-orbitronic experiments (such as harmonic Hall analysis of the SOT and unusual magnetoresistance), but also for the evaluation of the intrinsic band properties of novel magnetic materials (e.g., magnetic topological semimetals [1,4,5] and Kagome non-collinear antiferromagnets [49,62]) in heterostructures. Thus, it is of crucial importance and urgent need to clarify the scaling, mechanism, and impact of the anomalous Hall voltage in NM/FM heterostructures, particularly those with significant theoretically predicted spin and orbital Hall effects (e.g., Pt [6], Al, Mn, Ti [63,64]).

In this Letter, we perform a systematic study on seven different NM/magnet device series with varying material systems, layer thicknesses, resistivities, and spin/orbital Hall conductivities of the NM by combining transport experiments, analytical derivation, and finite-element analyses. We report the observation, universality, mechanism, and impacts of the scaling of the anomalous Hall voltage (V_{AH}/E) in magnetic heterostructures with d.

Received 4 August 2026; accepted 10 October 2026; published 9 November 2026

© 2026 Chinese Physical Society and IOP Publishing Ltd. All rights, including for text and data mining, AI training, and similar technologies, are reserved.

Check for updates

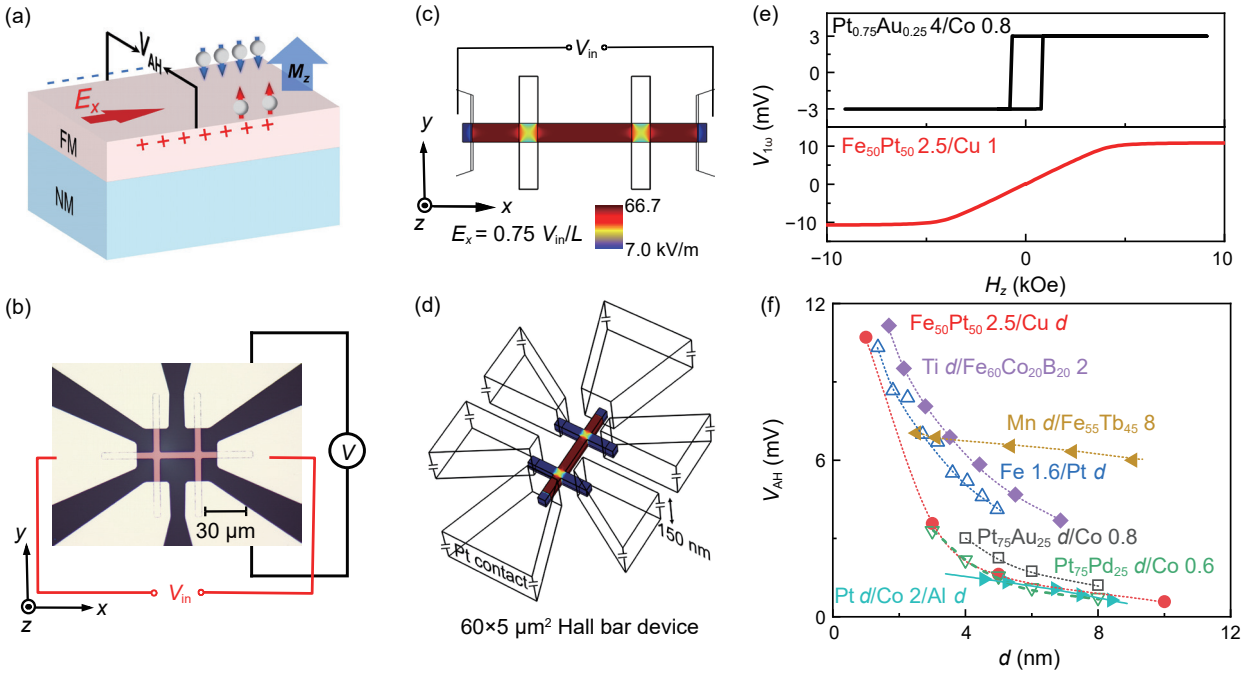

Fig. 1. (a) Schematic of the anomalous Hall effect. (b) Optical microscope image of the $Fe_{50}Pt_{50}$ 2.5/Cu 10 Hall device and measurement geometry of the anomalous Hall voltage. (c) The electric field E applied to the cross region is $0.75V_{in}/L$ when a voltage V_{in} is applied to the Hall bar with length L. (d) Device modeling and mesh division in the finite-element analysis. (e) $V_{1\omega}$ vs out-of-plane magnetic field H_z for the $Pt_{75}Au_{25}$ 4/Co 0.8 and the $Fe_{50}Pt_{50}$ 2.5/Cu 1. (f) Dependence on normal metal thickness of the anomalous Hall voltage for $Fe_{50}Pt_{50}$ 2.5/Cu *d*, Pt 5/Co 2/Al *d*, $Pt_{75}Au_{25}$ *d*/Co 0.8, $Pt_{75}Pd_{25}$ *d*/Co 0.6, Fe 1.6/Pt *d*, Mn *d*/$Fe_{55}Tb_{45}$ 8, and Ti *d*/$Fe_{60}Co_{20}B_{20}$ 2 heterostructures. E = 50 kV/m for the data in (c)–(f).

Devices and Methods

For this study, we sputter-deposited six NM/magnet bilayer series, i.e., $Pt_{75}Au_{25}$ 4–8/Co 0.8, $Pt_{75}Pd_{25}$ 3–8/Co 0.6, Fe 1.6/Pt 1.4–5, $Fe_{50}Pt_{50}$ 2.5/Cu 0–10, Ti 1.7–6.9/$Fe_{60}Co_{20}B_{20}$ 2, Mn 2.5–9.1/$Fe_{55}Tb_{45}$ 8, and a trilayer series Pt 5/Co 2/Al 3–9.6. Here, the numbers represent the layer thicknesses in nm. Pt [7, 65], $Pt_{75}Au_{25}$ [66], and $Pt_{75}Pd_{25}$ [67] are chosen as the heavy metals with strong spin Hall effect, Cu [19], while Ti [68−70], Mn [71], and Al [72] are the representatives of light metals with negligibly small spin Hall effect. Fe, Co, $Fe_{60}Co_{20}B_{20}$, and $Fe_{50}Pt_{50}$ are representative metallic ferromagnets (FMs), and $Fe_{55}Tb_{45}$ is a typical ferrimagnet [28]. Each sample is protected by a MgO 2/TaO_x 4 bilayer and fabricated into two-cross Hall bar devices with width (W) of 5 μm and length (L) of 60 μm [Fig. 1(b)]. Finally, Ti 5/Pt 150 contacts were deposited for transport measurements. For each series, V_{AH} is measured utilizing a lock-in amplifier (SR860, with a giant internal resistance of 10 MΩ) under a fixed sinusoidal electric field E, which helps to improve the signal-to-noise ratio, to avoid the influence of any current shunting, and to minimize the impact of Joule heating. Here, E of 50 kV/m is applied by the input voltage (V_{in}) of 4 V onto the 60 μm long Hall bar [Fig. 1(b)], i.e., $E = 0.75V_{in}/L$. The factor 0.75 arises from the lateral electric field spreading at the Hall crosses due to the presence of the detection leads [see Fig. 1(c) and Ref. [73]]. No thermal annealing was performed for the devices in this work to avoid uncertainty from interface variations.

Microscopic distributions of the electric current and fields in the NM/FM bilayers are simulated using finite-element analysis with a very small unit cell size of 0.2 nm×0.2 nm×0.2 nm (similar to that in Ref. [73]). The finite-element analysis follows the current continuity equation $\nabla \cdot \boldsymbol{j}_c + \partial\rho/\partial t = 0$ and the boundary condition of $\boldsymbol{n} \cdot \boldsymbol{j}_c = 0$, where $\boldsymbol{j}_c$ is the charge current density, ρ is the charge density, $\boldsymbol{n}$ is the normal direction of the device boundary. The analysis has taken into account the large Pt electrodes and the dimensions of the real device [Fig. 1(d)]. The SOT of the representative Hall devices of magnetic heterostructures are characterized using harmonic Hall voltage analysis to verify the mechanism and potential impact of the scaling of V_{AH} with the NM.

Universal Scaling of V_{AH} with the Normal Metal

The values of V_{AH} for the $Fe_{50}Pt_{50}$ 2.5/Cu *d*, Pt 5/Co 2/Al *d*, $Pt_{75}Au_{25}$ *d*/Co 0.8, $Pt_{75}Pd_{25}$ *d*/Co 0.6, Pt *d*/Fe 2.5, Mn *d*/$Fe_{55}Tb_{45}$ 8, and Ti *d*/$Fe_{60}Co_{20}B_{20}$ 2 are extracted from the dependence of $V_{1\omega}$ on the swept out-of-plane magnetic field (H_z) [Fig.1(e)]. As shown in Fig. 1(f), V_{AH} of each sample series decreases very rapidly at small *d* and then more gradually upon further increasing *d*. This observation suggests that it is a rather universal effect in which V_{AH} of magnetic heterostructures decreases upon increasing the thickness of the adjacent NM layer.

Finite-Element Simulations of the V_{AH} Scaling

The universal scaling of V_{AH} with the adjacent normal metal suggests that there is an intrinsic mechanism that causes the measured apparent anomalous Hall voltage of a magnetic layer to decrease with increasing the thickness of the adjacent NM layer. In general, there are two effects that could potentially affect the measurement of V_{AH}/E in magnetic heterostructures, i.e., the non-uniform distribution of electric field (equivalently, current) induced by current spreading and the charge screening effect of the NM acting as a series resistor. Here, we stress that the current flow in the NM due to the parallel resistor effect does not play any role in the V_{AH}/E [see Eq. (1)]. When the FM and NM are modeled as two parallel resistors under a constant electric field E (constant voltage source), the voltmeter would always measure the exact voltage output of the battery ($V_{AH,0}$), while $V_{AH,0}$ is unaffected by the NM according to Eq. (1).

As modeled in Fig. 2(a), when an excitation voltage V_{in} is applied from the top surfaces of the thick, highly conductive current electrodes (with a thickness of 150 nm and a resistivity of 10 μΩ·cm) to the thin magnetic heterostructures, strong spatial spreading of the current—and thus of the electric field—occors in the vertical direction. Qualitatively, such vertical spreading creates non-uniformity in the current distributions in the NM and magnetic layers, which further affects the experimentally measured values of V_{AH}. To evaluate this effect, we have performed finite-element analysis of the average volumetric integral of the longitudinal current density in the cross region

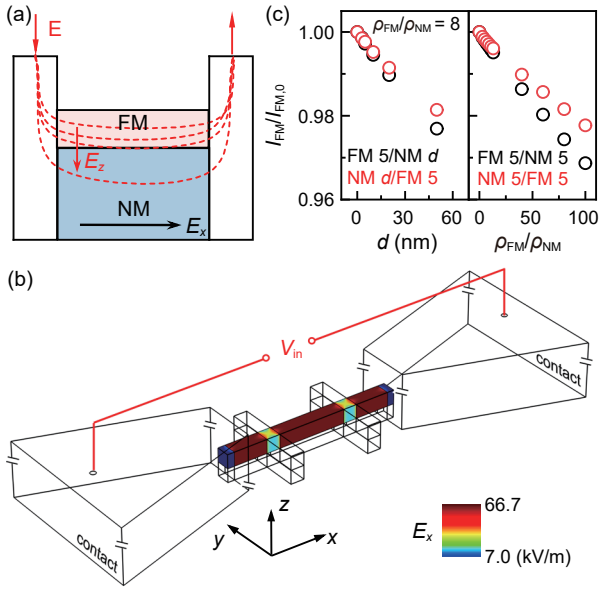

Fig. 2. (a) Schematic and (b) finite-element modeling of the electric field distributions in a NM/FM Hall bar with the thick electrical contacts. (c) Simulated results of $I_{FM}/I_{FM,0}$ vs the thickness of the NM (d) and the ratio of the resistivity of the FM and NM for a fixed input volage of V_{in} = 4 V (equivalently a fixed electric field of $E \approx 50$ kV/m).

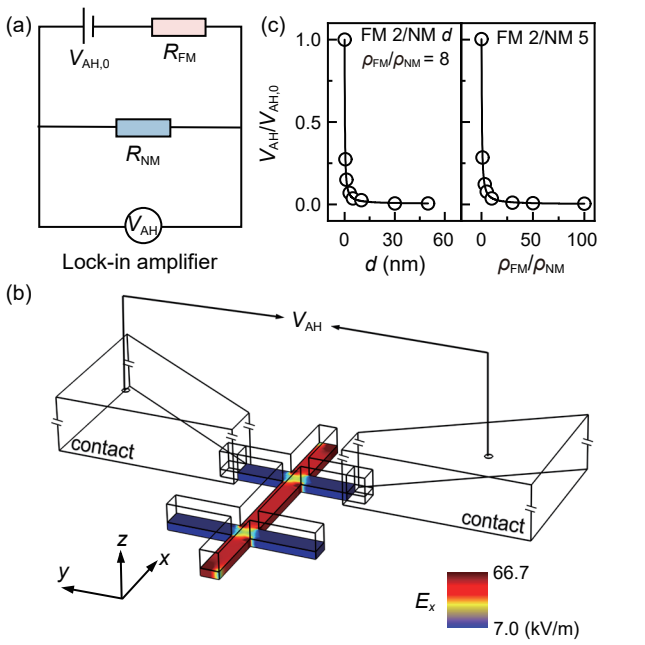

Fig. 3. (a) Schematic and (b) Finite-element modeling of the charge screening effect in NM/FM heterostructure on the detection of transverse voltage via the series-resistor effect. (c) Scaling of the simulated transverse voltage ($V_{AH}/V_{AH,0}$) for FM 2/NM d (ρ_{FM}/ρ_{NM} = 8) and FM 2/NM 5 with the thickness and resistivity of the NM.

of the FM (I_{FM}) in a bilayer Hall bar under a fixed input voltage of V_{in} = 4 V for the FM/NM [Fig. 2(b)] and NM/FM bilayers with opposite orders of the FM and the NM. In Fig. 2(c), we summarize the simulated I_{FM} in the FM layer normalized to the base value $I_{FM,0}$ for the FM 5/NM d and NM d/FM 5 bilayers as a function of d (ρ_{FM}/ρ_{NM} = 8) and ρ_{FM}/ρ_{NM} (d = 5 nm), respectively. Here, $I_{FM,0}$ represents the value of I_{FM} at d = 0 nm for d dependence and at ρ_{FM}/ρ_{NM} = 0 for the ρ_{FM}/ρ_{NM} dependence. I_{FM} decreases monotonically by less than 2.5% and 4%, respectively, even when d is dramatically increased from 0 nm to 50 nm. For the FM 5/NM 5 and NM 5/FM 5 bilayers with fixed layer thicknesses, I_{FM} also decreases by less than 2.5% and 3.5%, respectively, as ρ_{FM}/ρ_{NM} is increased from 0 to 100. These results suggest that the vertical current spreading effect only has negligible influence on the measurement of the anomalous Hall voltage of practical spintronic devices with ρ_{FM}/ρ_{NM} of <10 and t_{NM} < 10 nm.

The charge screening effect of the NM on the detection of the anomalous Hall voltage is schematically modeled in Fig. 3(a). In general, the FM and NM can be considered as two resistors in series. The FM generating the anomalous Hall voltage can be regarded as a battery with output $V_{AH,0}$, the two ends of which are connected simultaneously to the NM and the voltmeter (lock-in amplifier with an internal resistance of 10 MΩ). In this case, what the voltmeter measures is the voltage dropped across the NM rather than $V_{AH,0}$ of the FM. In other words, the experimentally measured value of V_{AH} from the NM is only a portion of that generated by the FM battery, while the voltage distribution in the FM is also significant. From the finite-element analysis [Fig. 3(b)], we simulated the Hall voltage between the two detection leads of a NM/FM Hall device under an electric field of E = 50 kV/m by taking into account the voltage distributions on the FM and the NM layers. As summarized in Fig. 3(c), the apparent values of V_{AH} from the measurement, i.e., the values of V_{AH} distributed on the NM, decrease dramatically towards vanishingly small value for the FM 2/NM d (ρ_{FM}/ρ_{NM} = 8) as d increases and for the FM 2/NM 5 as ρ_{FM}/ρ_{NM} increases, which is in good agreement with the experiments in Fig. 1(f).

Analytical Modeling of the V_{AH} Scaling

Based on the charge screening effect of the NM via the series-resistor model, the experimentally measured V_{AH} can be derived as

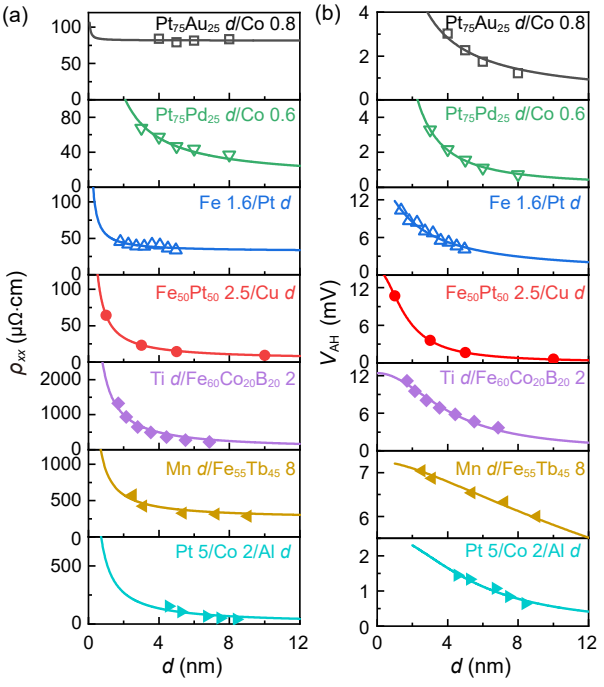

Fig. 4. Dependence on the NM thickness of (a) the resistivity of the NM and (b) the anomalous Hall voltage for $Pt_{75}Au_{25}$ d/Co 0.8, $Pt_{75}Pd_{25}$ d/Co 0.6, Fe 1.6/Pt d, Ti d/$Fe_{60}Co_{20}B_{20}$ 2, $Fe_{50}Pt_{50}$ 2.5/Cu d, Mn d/$Fe_{55}Tb_{45}$8, and Pt 5/Co 2/Al d. E = 50 kV/m for the data in (b).

$$V_{AH} = V_{AH,0}/(1+d\rho_{FM}/t\rho_{NM}), \quad (2)$$

where $V_{AH,0}$ is the anomalous Hall voltage of the FM in the absence of an adjacent NM layer. The magnitude of $V_{AH,0}$ is independent of the parameters of the NM. As indicated by the solid curves in Fig. 3(c), equation (2) fits well the scaling of V_{AH} with d and ρ_{FM}/ρ_{NM} from the finite-element analysis.

As shown in Fig. 4(a), for the various NM d/FM t bilayers with small d of a few nanometers, ρ_{NM} is not always constant but typically

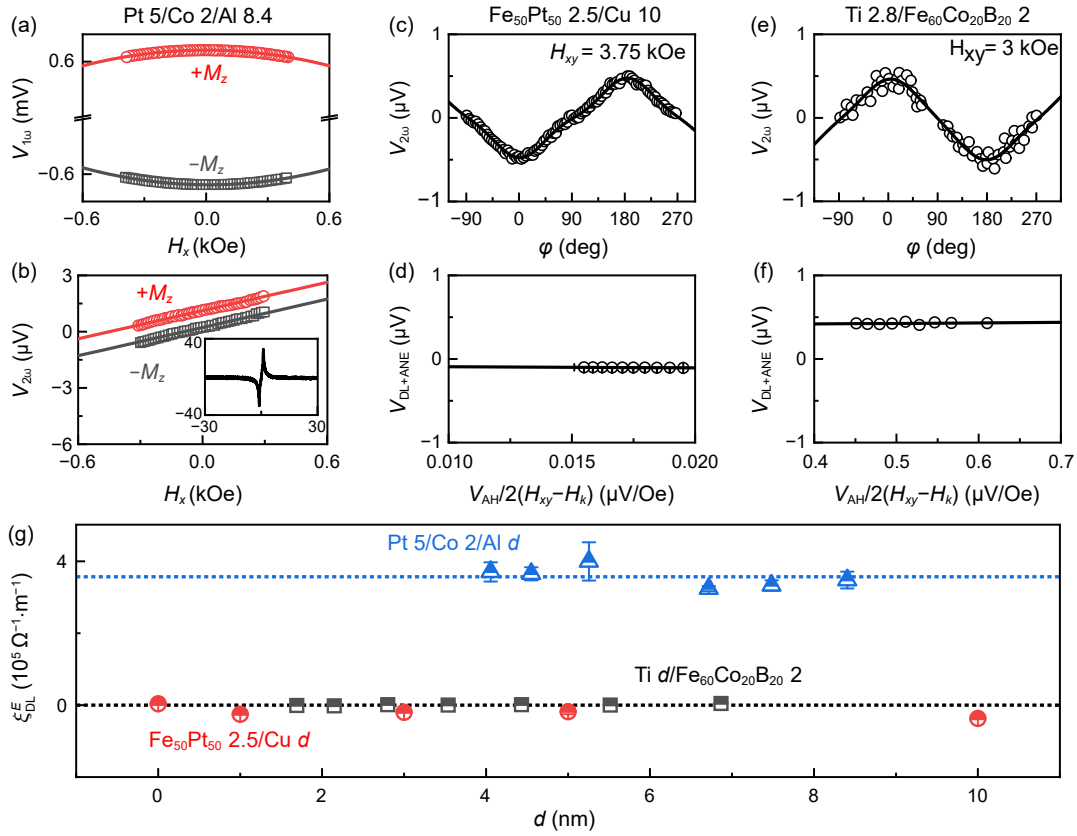

Fig. 5. Dependence on H_x of (a) the first-harmonic Hall voltage and (b) the second-harmonic Hall voltage for the Pt 5/Co 2/Al 8.4 with perpendicular magnetic anisotropy. (c) The second-harmonic Hall voltage vs azimuth angle (φ) of the in-plane magnetic field (H_{xy} = 3.75 kOe) and (d) $V_{\mathrm{DL+ANE}}$ vs $V_{\mathrm{AH}}/2(H_{xy} - H_k)$ for $Fe_{50}Pt_{50}$ 2.5/Cu 10. (e) The second harmonic Hall voltage vs φ (H_{xy} = 3 kOe) and (f) $V_{\mathrm{DL+ANE}}$ vs $V_{\mathrm{AH}}/2(H_{xy} - H_k)$ for the Ti 2.8/$Fe_{60}Co_{20}B_{20}$ 2. (g) Damping-like SOT efficiency per unit electric field for Pt/Co/Al d, $Fe_{50}Pt_{50}$/Cu d, and Ti d/$Fe_{60}Co_{20}B_{20}$ with different NM thickness.

Table 1. Spin and orbital Hall conductivities (σ_{SH}, σ_{OH}) of Pt, $Pt_{75}Au_{25}$, $Pt_{75}Pd_{25}$, Cu, Ti, Mn, and Al.

Material	σ_{SH} $(\hbar/2e)\ \Omega^{-1}\cdot\mathrm{cm}^{-1}$	σ_{OH} $(\hbar/2e)\ \Omega^{-1}\cdot\mathrm{cm}^{-1}$	Ref.
Pt	4000	5400	[62]
$Pt_{75}Au_{25}$	3600	-	[65]
$Pt_{75}Pd_{25}$	4500	-	[66]
Cu	60	2400	[62]
Ti	−80	7600	[63]
Mn	−260	18400	[62]
Al	60	−1400	[62]

increases upon decreasing d due to the interfacial scattering. Phenomenologically, the d dependence of ρ_{NM} follows

$$\rho_{\mathrm{NM}} = \rho_0 + \rho_{\mathrm{int}}/d, \tag{3}$$

where ρ_0 is the thickness-dependent resistivity contribution (including the bulk and interface resistances), and ρ_{int} parameterizes the scattering of electrons by the top and bottom interfaces of the NM. Interfacial scattering in a layer arises due to the layer thickness not being much greater than the electronic mean-free path (l_e) of that layer and varies with the thickness-to-l_e ratio of the same layer. Varying the NM thickness d directly varies the d/l_e ratio of the NM and thus the interfacial scattering at the two NM interfaces, but does not directly vary that of the adjacent FM layer. The influence of varying the NM thickness on ρ_{NM} of the FM layer is, at most, a secondary and much weaker effect. In addition, according to Eq. (2), any small decrease in the interfacial scattering of the FM with increasing NM thickness would lead to a small increase in the measured V_{AH}, and thus can be ignored in the following analyses of the universal decrease of V_{AH} with d.

In Fig. 4(a), the d dependence of the average resistivity of the NM is well fitted by Eq. (4), from which the values of ρ_0 and ρ_{int} for various NM/FM bilayers are subtracted. Taking interfacial scattering into account, equation (2) is rewritten as

$$V_{\mathrm{AH}} = V_{\mathrm{AH},0}/[1+d\rho_{\mathrm{FM}}/t(\rho_0+\rho_{\mathrm{int}}/d)]. \tag{4}$$

For the Pt d_{Pt}/Co t/Al d trilayers, equation (4) is modified as

$$V_{\mathrm{AH}} = V_{\mathrm{AH},0}/[1+d_{\mathrm{Pt}}\rho_{\mathrm{FM}}/t\rho_{\mathrm{Pt}}+d\rho_{\mathrm{FM}}/t(\rho_0+\rho_{\mathrm{int}}/d)]. \tag{5}$$

As shown in Fig. 4(b), the strong d dependence of the measured anomalous Hall voltage for all studied bilayers is well fitted by Eq. (4), regardless of the FM and NM types. The Al thickness dependence of the measured V_{AH} for the Pt/Co/Al is also well fitted using ρ_{Co} = 62.5 μΩ·cm and ρ_{Pt} = 33.8 μΩ·cm in Eq. (5).

Irrelevance to Angular Momentum Injection

Given the previous speculation of a strong modification of $V_{\mathrm{AH}}/I_{\mathrm{tot}}$ by spin angular momentum injected from the NM [52−57], we verify that the strong d dependence of the measured anomalous Hall voltage in NM/FM bilayers generally occurs even in the absence of any significant spin angular momentum injection from the thickness-varying NM to the FM (e.g., for Cu, Ti, Mn, and Al NMs listed in Table 1). We further probe angular momentum injection from the NM to the FM using the damping-like SOT efficiency (ξ^E_{DL}).

For this purpose, we perform harmonic Hall voltage analysis with E = 50 kV/m to quantify ξ^E_{DL} for three representative device series, i.e., perpendicularly magnetized Pt 5/Co 2/ Al d, in-plane magnetized $Fe_{50}Pt_{50}$ 2.5/Cu d, and in-plane magnetized Ti d /$Fe_{60}Co_{20}B_{20}$ 2. In these devices, the spin Hall effect is negligible in the thickness-varying light 3d NM layers (i.e., the Al, Cu, Ti) such that the true torque

values should remain independent of d.

For the Pt 5/Co 2/ Al d devices with perpendicular magnetic anisotropy (PMA), both $V_{1\omega}$ and $V_{2\omega}$ [Figs. 5(a) and 5(b)] are collected as a function of the swept in-plane longitudinal magnetic field (H_x) along the current direction. As shown in Fig. 5(a), $V_{1\omega}$ is a parabolic function of H_x as expected from the tilting of a macrospin, i.e.,

$$V_{1\omega}=V_{\mathrm{AH}}(1-H_x^2/2H_k^2), \tag{6}$$

where H_k is the perpendicular magnetic anisotropy field. In Fig. 5(b), $V_{2\omega}$ scales linearly with the H_x. We then determine the damping-like SOT field (H_{DL}) following formula [74]:

$$H_{\mathrm{DL}} = -2\frac{\partial V_{2\omega}}{\partial H_x}\Big/\frac{\partial^2 V_{1\omega}}{\partial H_x^2} - 2H_k\frac{V_{\mathrm{ANE}}}{V_{\mathrm{AH}}}, \tag{7}$$

where V_{ANE} is the anomalous Nernst voltage induced by the vertical thermal gradient and equals to the value of $V_{2\omega}$ when magnetization is fully aligned to the current direction by H_x that is much greater than H_k [see the inset of Fig. 5(b)].

For the in-plane magnetized $Fe_{50}Pt_{50}$ 2.5/Cu d and Ti d/$Fe_{60}Co_{20}B_{20}$ 2 devices, $V_{2\omega}$ is collected as a function of the azimuth angle (φ) of the in-plane magnetic field H_{xy} relative to the current direction [Figs. 5(c) and 5(e)]. $V_{2\omega}$ of an in-plane macrospin is given by [74]

$$V_{2\omega} = V_{\mathrm{DL+ANE}}\cos\varphi + V_{\mathrm{FL+Oe}}\cos\varphi\cos2\varphi + V_{\mathrm{PNE}}\sin2\varphi, \tag{8}$$

with

$$V_{\mathrm{DL+ANE}}=V_{\mathrm{AH}}H_{\mathrm{DL}}/2(H_{xy}-H_k)+V_{\mathrm{ANE}}. \tag{9}$$

Here, V_{PNE} is the planar Nernst voltage induced by the longitudinal thermal gradient. The fit of the φ dependence of $V_{2\omega}$ to Eq. (8) yields the values of $V_{\mathrm{DL+ANE}}$ and $V_{\mathrm{FL+Oe}}$ for each magnitude of H_{xy}. As shown in Figs. 5(d) and 5(f), the H_{DL} values of the in-plane magnetized devices are determined from the slope of the linear fits of $V_{\mathrm{DL+ANE}}$ vs $V_{\mathrm{AH}}/2(H_{xy}$ - $H_k)$ following Eq. (9). ξ^E_{DL} is then calculated following

$$\xi^E_{\mathrm{DL}} = (2e/\hbar)\mu_0 M_s t H_{\mathrm{DL}}/E, \tag{10}$$

where e is the elementary charge, $\hbar$ the reduced Planck constant, μ_0 the permeability of vacuum. As shown in Fig. 5(g), for all the device series, ξ^E_{DL} remains essentially constant despite the strong variation of V_{AH} with d. These results unambiguously reveal that the strong, universal scaling of the apparent anomalous Hall voltage with the adjacent NM thickness d is irrelevant to angular momentum injection from the NM to the FM. Note that the independence of ξ^E_{DL} on the thickness of the NM is consistent with the negligible orbital torque contributions from the Al, Ti, and Cu in previous reports [19,67–69,71].

Robustness of the Harmonic Hall Voltage Analysis

Since the damping-like SOT is identified from its interplay with the anomalous Hall voltage in the harmonic Hall voltage analyses, we discuss that the considerable misreading of V_{AH} due to the series-resistor effect of the NM does not affect the strength of the SOTs from the harmonic Hall voltage analysis. According to the series-resistor effect of the NM/FM bilayer and Eq. (2), any transverse voltages are lowered by the same factor of $1/(1+d\rho_{\mathrm{FM}}/t\rho_{\mathrm{NM}})$ compared to their true values. Thus, all the voltages in Eqs. (6)–(9), $V_{1\omega}$, $V_{2\omega}$, V_{ANE}, $V_{\mathrm{DL+ANE}}$, and V_{AH}, are lowered by the same factor, leading to no alteration to the values of H_{DL} and ξ^E_{DL} of PMA and in-plane magnetic devices as can be seen from Eqs. (7) and (9).

Conclusion

We have presented a systematic study on the observation, universality, mechanism, and impacts of the scaling of the anomalous Hall voltages in magnetic heterostructures with varying NM thicknesses by combining transport experiments, analytical derivation, and finite-element analyses. We show that the anomalous Hall voltage reduces universally and dramatically with the thickness of the adjacent nonmagnetic conducting layer, following Eqs. (4) and (5). We identify that the scaling arises only from the misreading of the invariant internal anomalous Hall voltage due to the series-resistor effect of the magnetic and nonmagnetic layers. The scaling remains strong and is well fitted by the series-resistor model, regardless of the strengths of the damping-like SOT and spin and orbital Hall conductivities of NMs, suggesting that such scaling of the measured anomalous Hall voltages cannot be attributed to angular momentum injection from the nonmagnetic layer to the magnetic layer. We have also discussed that the accuracy of the harmonic Hall voltage analyses of PMA and in-plane magnetized magnetic heterostructures are unaffected by the underestimation of the anomalous Hall voltage and other transverse voltages due to the series-resistor effect. These findings provide crucial information for understanding a variety of spintronic experiments involving the anomalous Hall and other transverse voltages.

Acknowledgements

This work was supported partly by the National Key Research and Development Program of China (Grant No. 2022YFA1204000), the Beijing Natural Science Foundation (Grant No. Z230006), and the National Natural Science Foundation of China (Grant Nos. 12274405 and 12304155).

References

[1] Li P, Koo J, Ning W, Li J, Miao L, Min L, Zhu Y, Wang Y, Alem N, Liu C, Mao Z, and Yan B 2020 *Nat. Commun.* **11** 3476
[2] Nakatani T, Kulkarni P D, Suto H, Masuda K, Iwasaki H, and Sakuraba Y 2024 *Appl. Phys. Lett.* **124** 070501
[3] Wang K, Zhang Y, and Xiao G 2020 *Phys. Rev. Appl.* **13** 064009
[4] Yang J, Shang Y, Liu X, Wang Y, Dong X, Zeng Q, Lyu M, Zhang S, Liu Y, and Wang B 2025 *Nat. Electron.* **8** 386
[5] Ni Y, Zhang Z, Nlebedim I C, and Jiles D C 2016 *IEEE Trans. Magn.* **52** 1
[6] Zhu L 2023 *Adv. Mater.* **35** 2300853
[7] Liu L, Lee O, Gudmundsen T, Ralph D, and Buhrman R 2012 *Phys. Rev. Lett.* **109** 096602
[8] Lau Y C, Betto D, Rode K, Coey J, and Stamenov P 2016 *Nat. Nanotechnol.* **11** 758
[9] Han J, Richardella A, Siddiqui S A, Finley J, Samarth N, and Liu L 2017 *Phys. Rev. Lett.* **119** 077702
[10] Yamanouchi M, Chiba D, Matsukura F, and Ohno H 2004 *Nature* **428** 539
[11] Sabri H, Carlson B E, Pershoguba S S, and Zang J 2025 *Phys. Rev. B* **111** 134433
[12] Maccariello D, Legrand W, Reyren N, Garcia K, Bouzehouane K, Collin S, Cros V, and Fert A 2018 *Nat. Nanotechnol.* **13** 233
[13] Wang L, Feng Q, Kim Y, Kim R, Lee K H, Pollard S D, Shin Y J, Zhou H, Peng W, and Lee D 2018 *Nat. Mater.* **17** 1087
[14] Zhang Y, Liu J, Dong Y, Wu S, Zhang J, Wang J, Lu J, Rückriegel A, Wang H, Duine R, Yu H, Luo Z, Shen K, and Zhang J 2021 *Phys. Rev. Lett.* **127** 117204
[15] Zhu L, Ralph D C, and Buhrman R A 2019 *Phys. Rev. Lett.* **122** 077201
[16] Wu L, Zhu K, Yue D, Tian Y, and Jin X 2016 *Phys. Rev. B* **93** 214418
[17] Zhu L and Ralph D C 2023 *Nat. Commun.* **14** 1778
[18] Lin X and Zhu L 2024 *Sci. China-Phys. Mech. Astron.* **67** 107511
[19] Avci C O, Garello K, Gabureac M, Ghosh A, Fuhrer A, Alvarado S F, and Gambardella P 2014 *Phys. Rev. B* **90** 224427
[20] Chi Z, Lau Y C, Xu X, Ohkubo T, Hono K, and Hayashi M 2020 *Sci. Adv.* **6** eaay2324
[21] Liu Q and Zhu L 2025 *Nat. Commun.* **16** 8660
[22] Zhu L, Liu Q, and Wang X 2025 *Natl. Sci. Rev.* **12** nwaf240
[23] Lin X, Zhu L, Liu Q, and Zhu L 2023 *Nano Lett.* **23** 9420
[24] Yan Z, Li Z, Zhu L, Lin X, and Zhu L 2025 *Chin. Phys. Lett.* **42** 090701
[25] Zhu L, Zhang X S, Muller D A, Ralph D C, and Buhrman R A 2020 *Adv. Funct. Mater.* **30** 2005201
[26] Liu Q, Lin X, and Zhu L 2023 *Adv. Sci.* **10** 2301409
[27] Liu L, Yu J, González-Hernández R, Li C, Deng J, Lin W, Zhou C,

Zhou T, Zhou J, Wang H, Guo R, Yoong H Y, Chow G M, Han X, Dupé B, Železný J, Sinova J, and Chen J 2020 *Phys. Rev. B* **101** 220402
[28] Liu Q, Zhu L, Zhang X S, Muller D A, and Ralph D C 2022 *Appl. Phys. Rev.* **9** 021402
[29] Zhang P, Liao L, Shi G, Zhang R, Wu H, Wang Y, Pan F, and Song C 2018 *Phys. Rev. B* **97** 214403
[30] Fan H, Jin M, Wu B, Wei M Z, Wang J, Shao Z, Yu C, Wen J, Li H, Li W, and Zhou T 2023 *Appl. Phys. Lett.* **122** 262404
[31] Saito Y, Ikeda S, Inoue H, and Endoh T 2023 *IEEE Trans. Magn.* **59** 1
[32] Zhang P, Chou C T, Yun H, McGoldrick B C, Hou J T, Mkhoyan K A, and Liu L 2022 *Phys. Rev. Lett.* **129** 017203
[33] Yoon J Y, Zhang P, Chou C T, Takeuchi Y, Uchimura T, Hou J T, Han J, Kanai S, Ohno H, Fukami S, and Liu L 2023 *Nat. Mater.* **22** 1106
[34] Wang Y, Xu Z, Zhu Y, Liu Q, Hu S, Jiang Y, and Chen L 2025 *Phys. Rev. Appl.* **24** 044011
[35] Shao Q, Tang C, Yu G, Navabi A, Wu H, He C, Li J, Upadhyaya P, Zhang P, Razavi S A, He Q, Liu Y, Yang P, Kim S K, Zheng C, Liu Y, Pan L, Lake R K, Han X, Tserkovnyak Y, Shi J, and Wang K L 2018 *Nat. Commun.* **9** 3612
[36] Wang X R, Wang C, and Wang X S 2023 *Sci. Rep.* **13** 309
[37] Miao B F, Huang S Y, Qu D, and Chien C L 2014 *Phys. Rev. Lett.* **112** 236601
[38] Han G, Lin X, Liu Q, Gong G, and Zhu L 2025 *Adv. Funct. Mater.* **36** e23908
[39] Yin X, Han G, Gong G, Kang J, Xiong C, and Zhu L 2025 *Chin. Phys. Lett.* **42** 110703
[40] Liu Q, Liu L, Xing G, and Zhu L 2024 *Nat. Commun.* **15** 2978
[41] Yu J, Qiu X, Wu Y, Yoon J, Deorani P, Besbas J M, Manchon A, and Yang H 2016 *Sci. Rep.* **6** 32629
[42] Liang S, Chen R, Cui Q, Zhou Y, Pan F, Yang H, and Song C 2023 *Nano Lett.* **23** 8690
[43] Liu Q and Zhu L 2026 *Sci. China-Phys. Mech. Astron.* **69** 117511
[44] Zhu L, Zhu L, Sui M, Ralph D C, and Buhrman R A 2019 *Sci. Adv.* **5** eaav8025
[45] Nagaosa N, Sinova J, Onoda S, MacDonald A H, and Ong N P 2010 *Rev. Mod. Phys.* **82** 1539
[46] Zhu L J, Pan D, and Zhao J H 2014 *Phys. Rev. B* **89** 220406(R)
[47] Zhu L J, Xiong P, and Zhao J H 2016 *Phys. Rev. B* **93** 195112
[48] Li Z, Lin X, Zou Y, Tan F, Zhu W, and Zhu L 2025 *Adv. Funct. Mater.* **35** e12048
[49] Nakatsuji S, Kiyohara N, and Higo T 2015 *Nature* **527** 212
[50] Zhu L, Zhu L, Liu Q, and Lin X 2023 *Phys. Rev. B* **108** 014420
[51] Zhang P, Xie K, Lin W, Wu D, and Sang H 2014 *Appl. Phys. Lett.* **104** 082404
[52] Sebe N, Pezo A, Krishnia S, Collin S, George J M, Fert A, Cros V, and Jaffrès H 2025 arXiv: 2512.18419 [cond-mat.mtrl-sci]
[53] Meng K K, Miao J, Xu X G, Wu Y, Zhao J H, and Jiang Y 2017 *Solid State Commun.* **255-256** 15
[54] Meng K K, Miao J, Xu X G, Xiao J X, Zhao J H, and Jiang Y 2016 *Phys. Rev. B* **93** 060406(R)
[55] Wang G L, Wu S X, Meng M, Li H W, Li D, Hu P, and Li S W 2018 *J. Appl. Phys.* **123** 113906
[56] Zhang Y Q, Sun N Y, Che W R, Shan R, and Zhu Z G 2016 *AIP Adv.* **6** 025214
[57] Kim S T, Chang J Y, Jeong Y C, Kim M, Lee A Y, Lee J, Choi Y S, Park S Y, Choe S B, Kim K W, Kim D H, and Je S G 2025 *Phys. Rev. B* **112** 014426
[58] Xu W J, Zhang B, Wang Z, Chu S S, Li W, Wu Z B, Yu R H, and Zhang X X 2008 *Eur. Phys. J. B* **65** 233
[59] Song Z, Zhu L, Yan Z, Liu Q, and Zhu L 2026 *Adv. Funct. Mater.* **36** e74926
[60] Liu Q and Zhu L 2025 *Adv. Sci.* **12** e07581
[61] Liu Q, Lin X, Nie Z, Yu G, and Zhu L 2024 *Adv. Mater.* **36** 2406552
[62] Ye L, Kang M, Liu J, von Cube F, Wicker C R, Suzuki T, Jozwiak C, Bostwick A, Rotenberg E, Bell D C, Fu L, Comin R, and Checkelsky J G 2018 *Nature* **555** 638
[63] Jo D, Go D, and Lee H W 2018 *Phys. Rev. B* **98** 214405
[64] Choi Y G, Jo D, Ko K H, Go D, Kim K H, Park H G, Kim C, Min B C, Choi G M, and Lee H W 2023 *Nature* **619** 52
[65] Zhu L, Zhu L, and Buhrman R A 2021 *Phys. Rev. Lett.* **126** 107204
[66] Zhu L, Ralph D C, and Buhrman R A 2018 *Phys. Rev. Appl.* **10** 031001
[67] Zhu L, Sobotkiewich K, Ma X, Li X, Ralph D C, and Buhrman R A 2019 *Adv. Funct. Mater.* **29** 1805822
[68] Zhu L and Buhrman R A 2021 *Phys. Rev. Appl.* **15** L031001
[69] Baek S C, Amin V P, Oh Y W, Go G, Lee S J, Lee G H, Kim K J, Stiles M D, Park B G, and Lee K J 2018 *Nat. Mater.* **17** 509
[70] Wang H L, Du C H, Pu Y, Adur R, Hammel P C, and Yang F Y 2014 *Phys. Rev. Lett.* **112** 197201
[71] Du C, Wang H, Yang F, and Hammel P C 2014 *Phys. Rev. B* **90** 140407(R)
[72] Zhang T, Zhu L, Yan Z, and Zhu L 2026 *Phys. Rev. B* **114** L020405
[73] Li Z, Liu Q, Zhu W, and Zhu L 2027 *Newton* **3** 100727
[74] Zhu L, Li J, Zhu L, and Xie X 2022 *Phys. Rev. Appl.* **18** 064052